EMBO reports

scientific report

Recognition of an intra-chain tandem 14-3-3 binding site within PKCε

Brenda Kostelecky[1,2], Adrian T. Saurin[2], Andrew Purkiss[1], Peter J. Parker[2,3] & Neil Q. McDonald[1,4+]

[1]Structural Biology, and [2]Protein Phosphorylation Laboratories, London Research Institute, Cancer Research UK, London, UK, [3]King's College London Division of Cancer Studies, Section of Cancer Cell Biology and Imaging, Guy's Hospital, London, UK, and [4]School of Crystallography, Birkbeck College, London, UK

The phosphoserine/threonine binding protein 14-3-3 stimulates the catalytic activity of protein kinase C-ε (PKCε) by engaging two tandem phosphoserine-containing motifs located between the PKCε regulatory and catalytic domains (V3 region). Interaction between 14-3-3 and this region of PKCε is essential for the completion of cytokinesis. Here, we report the crystal structure of 14-3-3ζ bound to a synthetic diphosphorylated PKCε V3 region revealing how a consensus 14-3-3 site and a divergent 14-3-3 site cooperate to bind to 14-3-3 and so activate PKCε. Thermodynamic data show a markedly enhanced binding affinity for two-site phosphopeptides over single-site 14-3-3 binding motifs and identifies Ser 368 as a gatekeeper phosphorylation site in this physiologically relevant 14-3-3 ligand. This dual-site intra-chain recognition has implications for other 14-3-3 targets, which seem to have only a single 14-3-3 motif, as other lower affinity and cryptic 14-3-3 gatekeeper sites might exist.

Keywords: 14-3-3; isothermal titration calorimetry; PKCε; crystal structure

EMBO reports (2009) **10**, 983–989. doi:10.1038/embor.2009.150

INTRODUCTION

The 14-3-3 family are phosphoserine/threonine binding modules that recognize proteins containing either a mode 1 motif (RSXpSXP, in which pS indicates phosphorylated serine) or mode 2 motif (RXF/YXpSXP; Muslin *et al*, 1996; Yaffe *et al*, 1997). 14-3-3 proteins can recognize non-phosphorylated targets and phosphoserine/threonine-containing sequences distinct from the canonical mode 1 and 2 motifs, generating a large and diverse array of potential substrates (Waterman *et al*, 1998; Fuglsang *et al*, 1999; Henriksson *et al*, 2002). 14-3-3 proteins are typically homodimeric and adopt a horseshoe-shaped structure (Liu *et al*, 1995; Xiao *et al*, 1995). The highly basic phosphoserine-binding pockets from each protomer face each other within the 14-3-3 dimer, allowing interactions from dimeric single-site partners as well as potentially two-site monomeric partners (Yaffe *et al*, 1997). Structural studies so far have focused on symmetric 14-3-3 complexes with either single-site peptides or dimeric protein partners (Yaffe *et al*, 1997; Petosa *et al*, 1998; Obsil *et al*, 2001; Ottmann *et al*, 2007).

The 14-3-3 isoforms show distinct regulatory functions towards various target proteins (reviewed by Bridges & Moorhead, 2005). Although several known 14-3-3 binding partners seem to contain a single binding motif, many have more than one confirmed 14-3-3 binding sites, including the serine kinase c-Raf, FOXO4, CDC25 and protein kinase C-ε (PKCε; Tzivion *et al*, 1998; Zeng *et al*, 1998; Obsil *et al*, 2003; Saurin *et al*, 2008). The presence of several 14-3-3 binding motifs within a single polypeptide raises the possibility of an intra-chain dual 14-3-3 binding site that engages both phosphoserine-binding clefts within a 14-3-3 dimer. Indeed, chemically linked 14-3-3 binding motifs have been shown to display positive cooperativity and enhanced binding compared with individual mono-phosphorylated motifs (Yaffe *et al*, 1997). For two-site dual 14-3-3 ligands, phosphorylation of one of the binding sites has been proposed to act as a 'gatekeeper' insofar as it is required for 14-3-3 binding but is not sufficient for full biological activity by itself (Yaffe, 2002). Despite considerable biological evidence suggesting that 14-3-3 might commonly use tandem intra-chain sites on binding partners (Obsil *et al*, 2003; Saurin *et al*, 2008), so far there has been no crystallographic or biophysical description of a biologically relevant tandem intra-chain 14-3-3 site.

We recently described the functional importance of a multi-phosphorylated PKCε V3 region that binds to 14-3-3 (Saurin *et al*, 2008). The actions of p38 and glycogen synthase kinase-3β (GSK3β) produce a mode 1 motif at residues 343–348 (RSKpSAP) of PKCε and autophosphorylation produces a divergent mode 2 motif at residues 364–370 (RKALpSFD) lacking proline at +2 and an aromatic residue at the −2 position (Durgan *et al*, 2008; Saurin *et al*, 2008; Fig 1A). The 14-3-3 interaction mediated by these motifs is crucial for the exit from cytokinesis, as shown by PKCε mutants S346A/S368A or R343A, which prevent the ability of

[1]Structural Biology, and [2]Protein Phosphorylation Laboratories, London Research Institute, Cancer Research UK, 44 Lincoln's Inn Fields, London WC2A 3PX, UK [3]King's College London Division of Cancer Studies, Section of Cancer Cell Biology and Imaging, New Hunt's House, Guy's Hospital, St Thomas Street, London SE1 1UL, UK [4]School of Crystallography, Birkbeck College, Malet Street, London WC1E 7HX, UK [+]Corresponding author. Tel: +44 (0)207 269 3259; Fax: +44 (0)207 269 3258; E-mail: neil.mcdonald@cancer.org.uk

Received 20 March 2009; revised 8 May 2009; accepted 29 May 2009; published online 7 August 2009

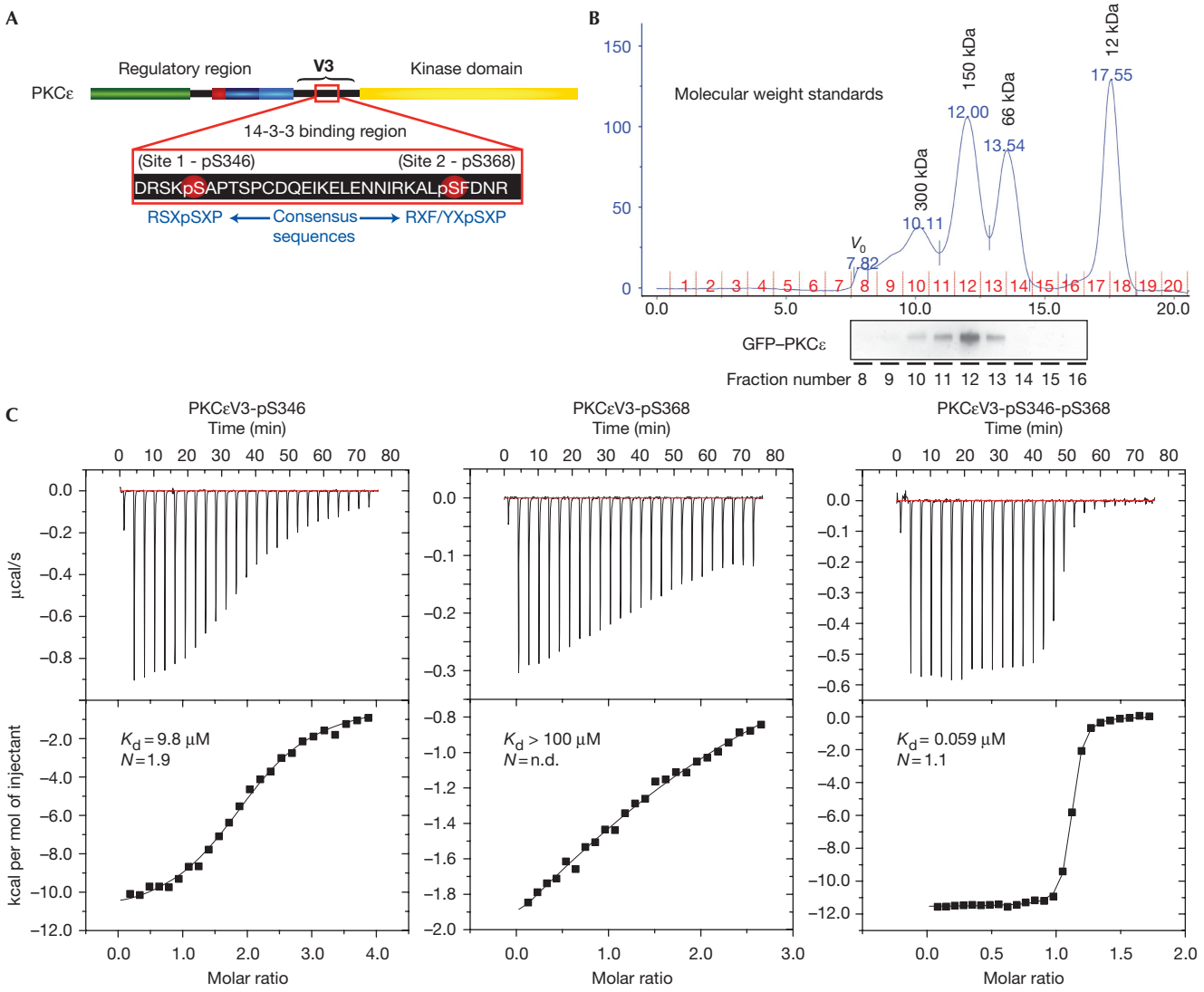

Fig 1 | Stoichiometry and thermodynamics of the 14-3-3–PKCε interaction. (**A**) Schematic showing PKCε primary structure, 14-3-3 phosphoserine-binding motifs and idealized 14-3-3 consensus sequences underneath. (**B**) The 14-3-3ζ–GFP-PKCε complex migrates by size exclusion chromatography with an apparent molecular weight that is consistent with a stoichiometry of one GFP–PKCε monomer (110 kDa) to one 14-3-3ζ dimer (58 kDa). (**C**) Isothermal titration calorimetry experiments showing binding curves for PKCεV3 monophosphopeptides and diphosphopeptide. Raw data are shown in the top panels with fitted curves below. GFP, green fluorescent protein, PKCε, protein kinase C-ε.

PKCε to recover cytokinesis defects after PKCε knockout or knockdown (Saurin *et al*, 2008). Here, we report a structural and thermodynamic characterization of the PKCε V3 region, a physiological 14-3-3 ligand that contains tandem intra-chain 14-3-3 binding sites with a 'gatekeeper' phosphorylation site as first postulated by Yaffe (2002).

RESULTS AND DISCUSSION

14-3-3ζ–PKCε complex stoichiometry

To confirm the composition of a complex containing a full-length PKCε bound to 14-3-3ζ, we assembled green fluorescent protein (GFP)-tagged PKCε with 14-3-3ζ according to published protocols (Saurin *et al*, 2008). The complex was then fractionated by using size exclusion chromatography and probed with a PKCε antibody, showing a molecular weight of 150 kDa consistent with a 14-3-3ζ dimer bound to one molecule of PKCε (Fig 1B), which is in agreement with published data for a 14-3-3β–PKCε complex (Saurin *et al*, 2008).

We then investigated the stoichiometry of a smaller analogous complex between 14-3-3ζ and a biotinylated PKCε V3 region diphosphopeptide (PKCεV3-b-pS346-pS368) spanning residues 342–372. By using an avidin displacement assay, we found that this complex showed a stoichiometry of 0.96 (±0.15) peptide molecules per 14-3-3 dimer (see Methods). Furthermore, it was possible to disrupt the association of PKCε and 14-3-3 in cell extracts by adding the PKCεV3-b-pS346-pS368 peptide (supplementary Fig S1 online). Thus, the diphosphorylated PKCε V3 peptide retains the essential features of the intact 14-3-3–PKCε complex.

Table 1 | PKCε V3 peptide binding constants for 14-3-3ζ

Peptide	K_d* (μM)	$N^{\dagger}$
PKCεV3-n	ND	–
PKCεV3-pS346 (site 1)	9.8 ± 0.44	1.9 ± 0.0083
PKCεV3-pS368 (site 2)	> 100	–
PKCεV3-pS346-pS368	0.059 ± 0.0030	1.1 ± 0.0011
PKCεV3-pS346-pS350-pS368	2.0 ± 0.20	1.5 ± 0.013
PKCεV3-site2-site2	0.75 ± 0.051	1.3 ± 0.0042
PKCεV3-site1-site1‡	0.00058 ± 0.00043 0.0072 ± 0.0045	0.69 ± 0.066 0.49 ± 0.062
PKCεV3-G6	6.9 ± 0.53	2.0 ± 0.021
PKCεV3-G10	0.12 ± 0.0090	0.88 ± 0.0023
PKCεV3-G14	0.13 ± 0.012	0.93 ± 0.0029

ND, not detectable; PKCε, protein kinase C-ε. *$K_D = 1/K_A$. †N = stoichiometry of binding (peptide to 14-3-3 dimer). ‡Both K_{D1} and K_{D2} estimates possible, see supplementary information online. Each experiment was carried out for a minimum of three times on independent samples.

Tandem phosphoserine sites enhance 14-3-3 binding

To probe the thermodynamics of the 14-3-3–PKCε interaction, we synthesized PKCε-V3 region peptides spanning residues 342–372 and characterized them using isothermal titration calorimetry (ITC). The peptides corresponded to monophosphorylated (PKCεV3-pS346 and PKCεV3-pS368), diphosphorylated (PKCεV3-pS346-pS368) or unphosphorylated (PKCεV3-n) species. The ITC results are summarized in Table 1. The monophosphorylated PKCεV3-pS346 (defined hereafter as site 1) showed a modest affinity (dissociation constant $K_d = 9.8\,\mu M$), consistent with it conforming to an optimal mode 1 14-3-3 binding motif. By contrast, binding of the PKCεV3-pS368 peptide (defined hereafter as site 2) was too weak to accurately determine the dissociation constant. The unphosphorylated peptide PKCεV3-n showed no detectable binding. Combining site 1 and site 2 within a diphosphopeptide markedly enhanced its affinity for 14-3-3 ($K_d = 59\,nM$), resulting in a 166-fold increase in affinity over site 1 alone (Fig 1C). This shows that Ser 368 of site 2 shows characteristics of a gatekeeper phosphorylation site, being necessary for high-affinity binding but with almost no intrinsic affinity for 14-3-3 by itself. The apparent stoichiometry from our ITC experiments indicates that a 14-3-3 dimer interacts with two molecules of PKCεV3-pS346 site-1 phosphopeptide and one molecule of PKCεV3-pS346-pS368 diphosphopeptide (Table 1). The bidentate interaction is likely to be the only stable conformation *in vivo*, as mutation of either binding site renders the 14-3-3–PKCε interaction undetectable (Saurin *et al*, 2008).

To create a GSK3β recognition motif (SXXXpS; Fiol *et al*, 1990) and hence trigger phosphorylation at Ser 346, a priming phosphorylation is required at Ser 350 (Saurin *et al*, 2008). The peptide PKCεV3-pS346-pS350-pS368 was therefore synthesized to mimic the triphosphorylated V3 region of PKCε. PKCεV3-pS346-pS350-pS368 showed a K_d of 2.0 μM for 14-3-3 (supplementary Fig S2A online), a significantly higher affinity than PKCεV3-pS346 site 1 but still 34-fold weaker than that of the diphosphopeptide (Table 1). The weaker affinity indicates that this phosphorylation compromises the high-affinity tandem interaction with 14-3-3. Consequently, selective dephosphorylation of Ser 350 might be important for 14-3-3 activation of PKCε, although the phosphorylation state of Ser 350 during cytokinesis is uncharacterized.

To determine whether two weak tandem sites are sufficient to produce an enhanced 14-3-3 binding interaction, we carried out similar ITC experiments on a diphosphopeptide with the site-2 sequence RKALpSFD at both ends of the peptide (PKCεV3-site2-site2). This peptide had a K_d of 750 nM and is a significant improvement in affinity over the virtually undetectable binding of a single pS368 site 2. Furthermore, it is almost tenfold weaker than for the PKCεV3-pS346-pS368 diphosphopeptide. By contrast, ITC binding curves obtained from a peptide with two optimal 14-3-3 binding sites (with sequence RSKpSAP, designated PKCεV3-site1-site1) showed approximately 100-fold higher affinity than PKCεV3-pS346-pS368 binding. This high affinity interaction was strong enough to observe two separate binding events ($K_{d1} = 0.58\,nM$ and $K_{d2} = 7.2\,nM$; supplementary Fig S2B,C). These experiments lead us to conclude that the affinity of the PKCεV3 region has been selected to allow regulated 14-3-3 binding through gatekeeper phosphorylation, rather than to maximize 14-3-3 affinity.

Structure of a 14-3-3–diphosphopeptide complex

To investigate this interaction further we then crystallized and determined the structure of the 14-3-3–PKCεV3-pS346-pS368 complex at a resolution of 2.2 Å (see supplementary Table S1 online for details). Crystals contained two 14-3-3 dimers within the asymmetric unit, each of which bound a phosphopeptide ligand. As one 14-3-3 dimer showed clearer electron density for the bound diphosphopeptide, we used this complex for the structural description below. Fortuitously, we did not observe an admixture of the diphosphopeptide bound in both possible orientations to a 14-3-3 dimer.

The refined model includes mainchain atoms for PKCεV3 residues 343–347 (site 1) and 365–372 (site 2), including both pS346 and pS368. Side-chain density for residues Lys 345 and Leu 367 assisted with the assignment of pS346 and pS368 to each 14-3-3 protomer (Fig 2A). The presence of an ordered site 2, despite its almost undetectable affinity for 14-3-3 by itself, indicates that it is highly likely to be connected to site 1 through the same diphosphopeptide, which is consistent with our thermodynamic data and the apparent stoichiometry of the complex. However, the intervening linker sequence (residues 348–364) is not ordered, leaving a gap of 32 Å from the end of site 1 to the start of site 2 (Fig 2B). A tight turn is likely to connect site 1 and site 2, as the PKCεV3 site-1 sequence has a consensus proline (Pro 348) at the +2 position, previously shown to kink the path of the peptide mainchain by 180° (Rittinger *et al*, 1999).

The r.m.s. difference for site 1 compared with a mode 1 structure (0.4 Å over 5 Cα for Protein Data Bank (PDB) code 1QJB) is lower than that of site 2 compared with a mode 2 structure (0.9 Å over 7 Cα for PDB code 1QJA), reflecting the greater similarity of site 1 to a consensus 14-3-3 sequence (Fig 3B). The 14-3-3ζ dimer is similar to previously reported 14-3-3 structures (supplementary Fig S3 online).

The 14-3-3 side chains coordinating each phosphoserine moiety include $R56^{14\text{-}3\text{-}3}$, $R127^{14\text{-}3\text{-}3}$ and $Y128^{14\text{-}3\text{-}3}$ as previously

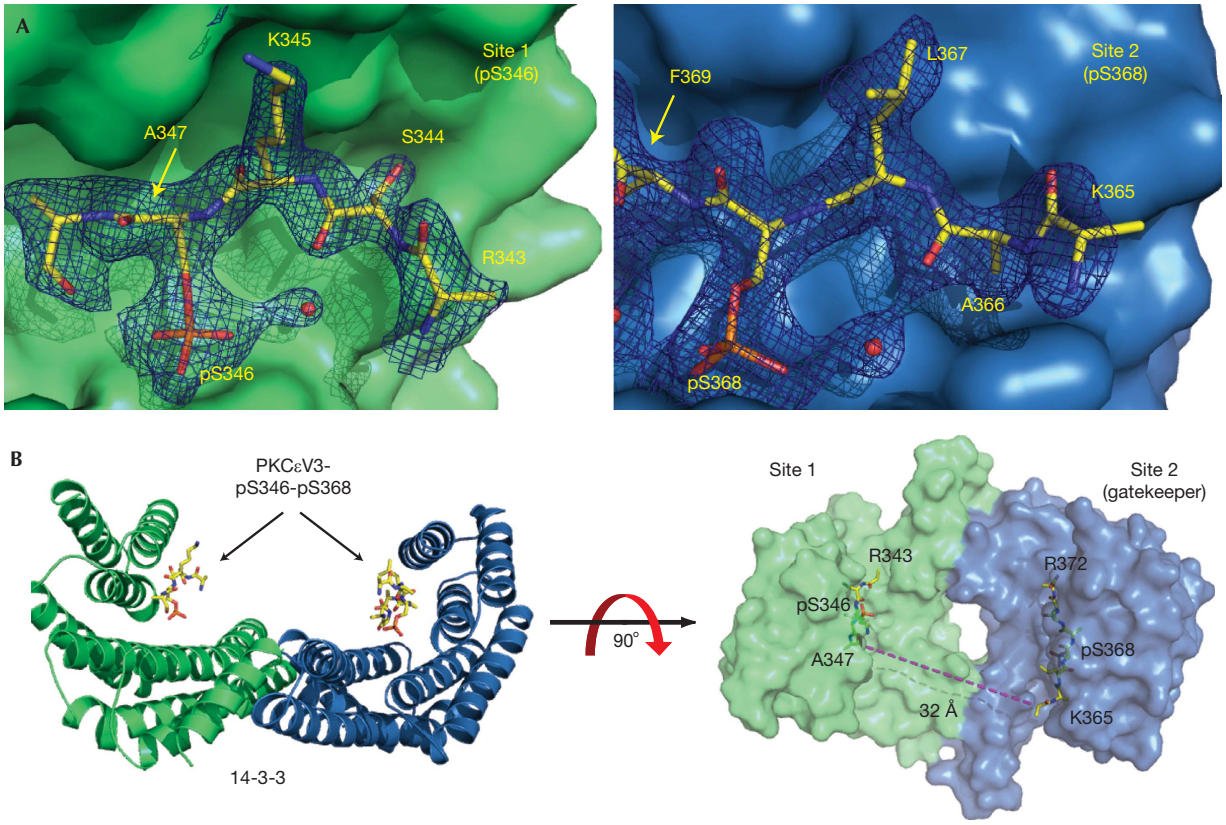

Fig 2 | Structure of the 14-3-3–PKCεV3 complex. (**A**) The electron density (2mFo-DFc contoured at $\sigma = 1.2$) for the 14-3-3–PKCεV3-pS346-pS368 diphosphopeptide complex is shown. (**B**) Surface representation of the 14-3-3 dimer (protomers are shown in blue and green, respectively) with the PKCεV3-pS346-pS368 peptide shown as sticks in yellow, and the location and distance spanned by the missing connecting linker indicated. The figure was prepared using PyMOL (Delano, 2002). PKCε, protein kinase C-ε.

reported for other phosphoserine peptides (Fig 3A). The side chain of K49$^{14\text{-}3\text{-}3}$ also coordinates pS368 in site 2 but is poorly ordered beyond the Cγ atom for site 1 and was omitted from the final model. Side chains of N224$^{14\text{-}3\text{-}3}$ and N173$^{14\text{-}3\text{-}3}$ form a hydrogen bond with mainchain atoms from the −1 and +1 residues relative to each phosphoserine, which is also consistent with previous 14-3-3 structures (Yaffe *et al*, 1997).

The greater affinity of 14-3-3 for a PKCεV3-pS346 site-1 peptide over a PKCεV3-pS368 site-2 peptide can be rationalized by the greater number of hydrogen bonds formed by interaction with the site-1 peptide (Fig 3A). These include hydrogen bonds from the E180$^{14\text{-}3\text{-}3}$ side chain to S344$^{PKC\varepsilon V3}$ mainchain nitrogen and the S344$^{PKC\varepsilon V3}$ side chain to Nε of W228$^{14\text{-}3\text{-}3}$. The latter interaction is not possible in site 2 as the serine is replaced by alanine (Ala 367). Furthermore, K345$^{PKC\varepsilon V3}$ from site 1 forms a salt bridge with D223$^{14\text{-}3\text{-}3}$. For the site 2-bound protomer, the D223$^{14\text{-}3\text{-}3}$ side chain is torsioned away from the binding pocket, presumably because the equivalent site 2 residue to Lys 345 is Leu 367 (Fig 3A). Neither the R343$^{PKC\varepsilon V3}$ nor the R364$^{PKC\varepsilon V3}$ side chain is included in the final model, similar to several other reported peptide-bound 14-3-3 structures, however, a role in phosphoserine coordination is likely (Yaffe *et al*, 1997; Petosa *et al*, 1998).

The weaker affinity of the triphosphorylated PKCεV3-pS346-pS350-pS368 peptide for 14-3-3 might be explained by the predicted tight turn induced by P348$^{PKC\varepsilon V3}$, placing pS350$^{PKC\varepsilon V3}$ in close proximity to the pS346$^{PKC\varepsilon V3}$ binding pocket and thereby potentially perturbing pS346$^{PKC\varepsilon V3}$ coordination by 14-3-3.

A shortened linker abolishes high-affinity binding

To determine how linker length influences 14-3-3–PKCε binding, residues 350–363 of PKCεV3-pS346-pS368 were replaced with 6, 10 and 14 glycine residues, (peptides PKCεV3-pS346-G6-pS368, PKCεV3-pS346-G10-pS368 and PKCεV3-pS346-G14-pS368). This was predicted to give maximal linker lengths of 22.8, 38 and 58.2 Å, respectively (calculated from a model peptide in an extended conformation). ITC binding curves showed that the G14 and G10 linked peptides retained high-affinity binding for 14-3-3 ($K_d = 120$ and 130 nM, respectively), consistent with linker lengths greater than 32 Å allowing two-site binding (Fig 2B). By contrast, the G6 linked peptide binding affinity ($K_d = 6.9\,\mu M$) was comparable with that measured for the PKCεV3-pS346 monophosphorylated peptide (Table 1; supplementary Fig S4 online). We also observed a concomitant increase in stoichiometry from one to two molecules of the G6 linker peptide bound per 14-3-3 dimer. These data indicate that a minimal linker

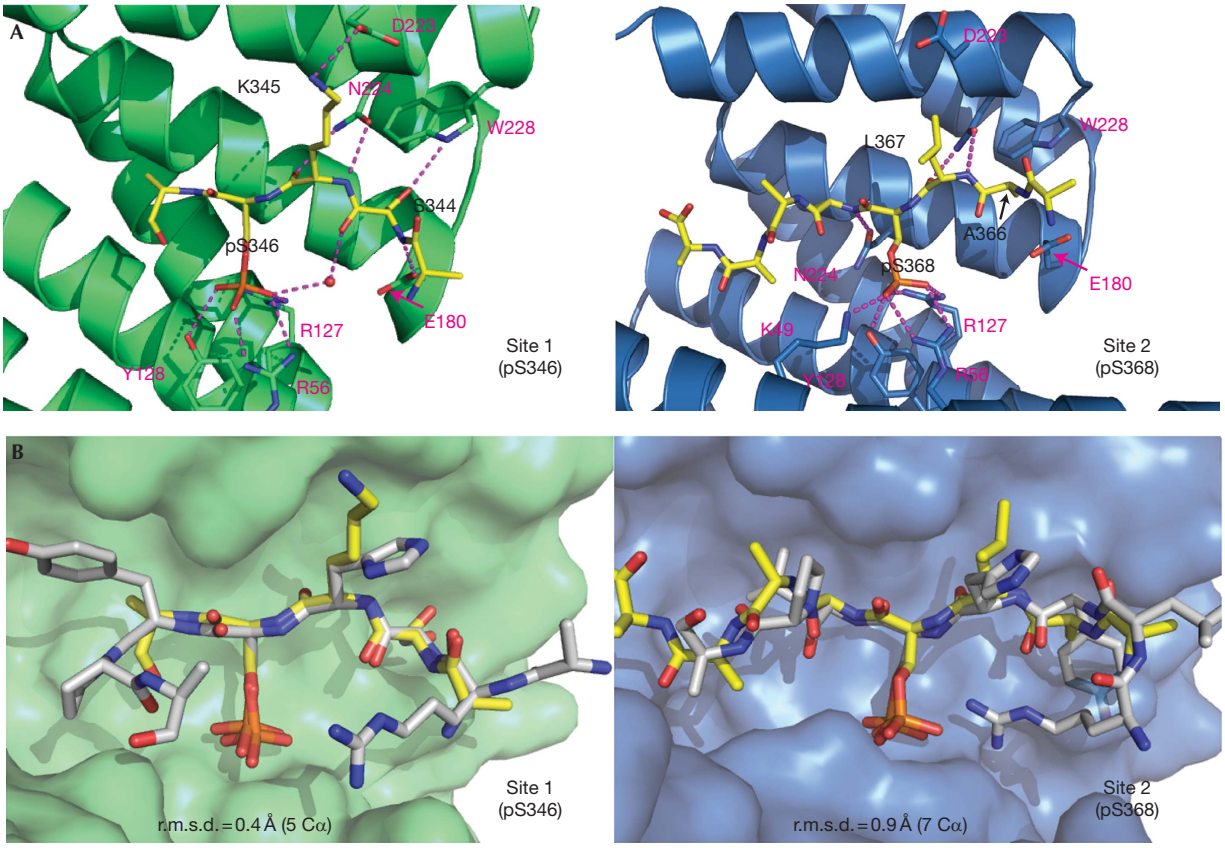

Fig 3 | Close-up of the molecular contacts made by each phosphoserine binding site and structural comparisons. (**A**) Hydrogen bonds are shown for site 1 (left panel) and site 2 (right panel) with selected interaction residues labelled in pink (14-3-3) and black (PKCε). (**B**) Comparison of the PKCεV3 site 1 with a mode 1 14-3-3 peptide (left panel, grey, PDB code 1QJB) and site 2 with a mode 2 peptide (right panel, grey, PDB code 1QJA). PKCεV3-pS346-pS368 is shown in yellow, 14-3-3 chain A is green and chain B is blue. Residue numbers are labelled as in panel (**A**). The figure was prepared using PyMOL (Delano, 2002). PDB, protein data bank; PKCε, protein kinase C-ε.

sequence of approximately ten residues is required between the two half sites to generate a tandem intramolecular 14-3-3 site. The PKCε linker is somewhat longer and has a predicted short helix (Ile 356 to Leu 367) and several acidic residues that might influence linker conformation after PKCε phosphorylation.

Wider implications for tandem 14-3-3 binding sites

Previous studies by Yaffe *et al* (1997) chemically linked two identical 14-3-3 sites from c-Raf to mimic a tandem intra-chain 14-3-3 site. This synthetic substrate showed a 30-fold higher affinity for 14-3-3 over a single 14-3-3 site. This led to the 'gatekeeper' phosphorylation hypothesis for biologically relevant tandem-site 14-3-3 ligands (Yaffe, 2002). Our data provide compelling evidence for this postulate by showing that a divergent 14-3-3 site is required for high-affinity binding, but has a barely detectable interaction on its own. Our asymmetrically bound 14-3-3 ligand structure reveals the conformation of such a gatekeeper site in contrast to previous symmetric 14-3-3–peptide structures (Fig 4A). We also show that the affinity of the tandem 14-3-3 site can be attenuated by a third phosphorylation, allowing further regulatory inputs to potentially alter complex formation and PKCε activation. PKCε thus provides a good example of how divergence from a consensus 14-3-3 motif within a gatekeeper site opens up the target to a wider range of modulators, either serine/threonine kinases or phosphatases, that control 14-3-3 binding. This is in marked contrast to the more limited array of regulators that can act on a strict consensus 14-3-3 site.

The implications of two-site intra-chain 14-3-3 binding extend beyond PKCε given that many confirmed 14-3-3 targets contain multiple 14-3-3 binding motifs, some of which conform to a mode 1/mode 2 consensus but many of which do not (Fig 4B). A similar affinity enhancement might be anticipated in these examples, in which a weaker divergent 14-3-3 site is present. For multi-site 14-3-3 ligands such as c-Raf the situation is likely to be more complicated. For example, c-Raf contains two optimal 14-3-3 binding sites and more than 10 sequences, which could form imperfect 14-3-3 motifs. Although c-Raf is able to bind to dimerization-deficient 14-3-3 mutants, its activation is impaired (Tzivion *et al*, 1998), suggesting that tandem binding indeed has a crucial role in regulating the interaction. Importantly, many of the known 14-3-3 targets with a single reported 14-3-3 interaction motif possibly contain as yet unidentified motifs crucial to their association with 14-3-3. Our data, therefore, suggest a significant role for two-site intra-chain binding across a spectrum of 14-3-3

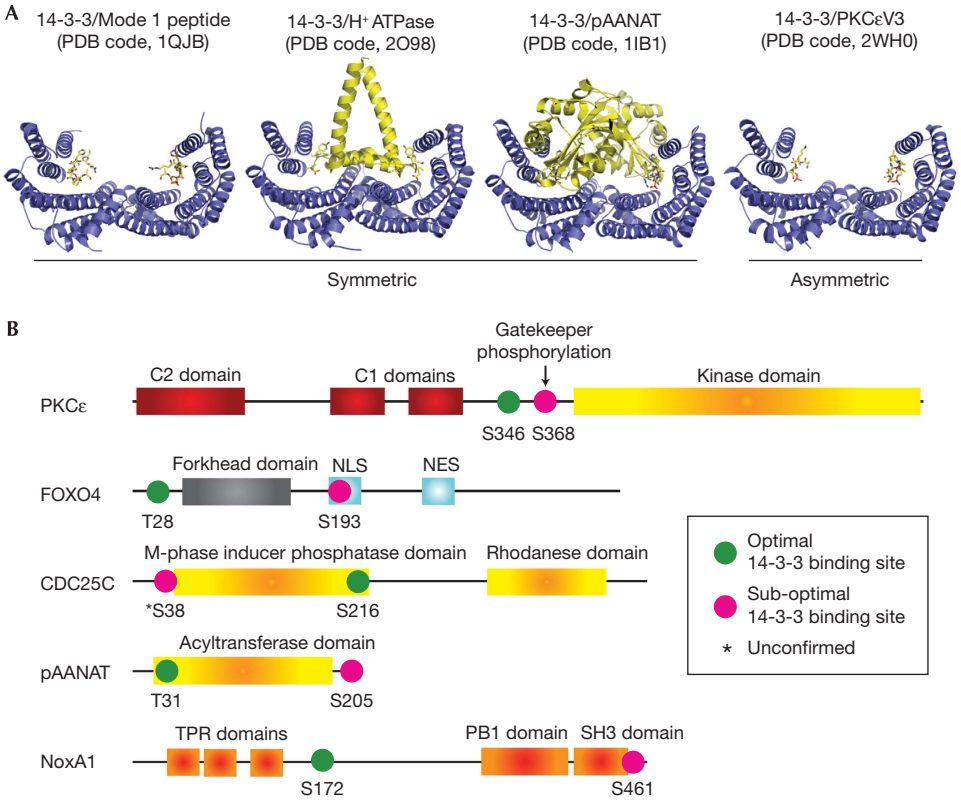

Fig 4 | Distinct binding modes for 14-3-3 partner proteins and selected examples of proteins with known two-site intra-chain 14-3-3 binding sites. (**A**) Structures of inter-chain (symmetric) complexes with a 14-3-3 dimer (blue ribbon) compared with the intra-chain (asymmetric) structure described for the PKCεV3 ligand. (**B**) The domain structure and location of consensus and divergent 14-3-3 sites within selected intra-chain two-site 14-3-3 partners. Optimal motifs are defined as those containing at least three out of four consensus mode 1 or mode 2 residues (Peng *et al*, 1997; Obsil *et al*, 2003; Ganguly *et al*, 2005; Kim *et al*, 2007; Saurin *et al*, 2008). PDB, protein data bank; PKCε, protein kinase C-ε.

interaction partners, and highlight the importance of identifying cryptic motifs and assessing their roles in a physiological setting.

METHODS

Protein purification. BL21(DE3) *Escherichia coli* cells expressing hexa-histidine-tagged 14-3-3ζ (His-14-3-3) were induced at OD_{600} 0.8 with 0.4 mM isopropyl-β-D-1-thiogalactopyranoside for 5 h at 37 °C. Cells were lysed in buffer A (20 mM HEPES (pH 7.4), 100 mM NaCl, 1 mM tris (2-carboxyethyl) phosphine) with complete EDTA-free protease inhibitors (Roche Diagnostics, West Sussex, UK) by sonication. The supernatant was applied to a Ni^{2+}-loaded HiTrap chelating column (GE Healthcare, Buckinghamshire, UK). His-14-3-3 was eluted with buffer A with 200 mM imidazole (pH 7.4). Gel filtration was carried out on a HiLoad 26/60 Superdex 200 column (GE Healthcare) in buffer A.

Stoichiometry measurements. Human embryonic kidney-293 cells producing tetracycline-induced GFP–PKCε were treated with 400 nM phorbol-12-myristate-13-acetate and 100 nM calyculin A phosphatase inhibitor for 20 min. Cell lysate was added to Ni–nitrilotriacetic acid beads pre-bound to 14-3-3ζ. The 14-3-3ζ–PKCε complex was eluted with imidazole and separated on a Superdex 200 10/30 GL column (GE Healthcare) in 50 mM Tris (pH 7.5), 150 mM NaCl, 0.5% TritonX-100 and 10 mM NaF. Molecular-weight standards were used as references. Eluted 14-3-3ζ–PKCε complex was detected using Western blotting with a PKCε antibody (Santa Cruz, Santa Cruz, CA, USA).

Peptide stoichiometry was determined using the EZ Biotin Quantitation Kit (Pierce Chemicals, IL, USA). A fivefold excess of biotinylated PKCεV3-b-pS346-pS368 peptide was incubated with 14-3-3ζ followed by gel filtration in PBS buffer (5.3 mM Na_2HPO_4, 1.8 mM KH_2PO_4, 140 mM NaCl, 3.5 mM KCl, (pH 7.2)). The complex was added to 4′-hydroxyazobenzene-2-carboxylic acid–avidin solution in PBS. The absorbance was measured at 500 nm and the biotin/protein ratio calculated according to the manufacturer's instructions.

ITC. His-14-3-3 and HPLC-purified synthetic peptides were dialysed overnight in PBS + 1 mM tris (2-carboxyethyl) phosphine. Peptides were injected in 1.4 μl increments into 200 μl 14-3-3ζ using concentrations ranging from 100 to 1,400 μM injectant and from 10 to 100 μM in the cell. All measurements were conducted a minimum of three times on independent samples in an iTC200 (Microcal, Milton Keynes, UK).

Crystallization. The 14-3-3ζ–PKCεV3-pS346-pS368 complex was crystallized by vapour diffusion. A total of 1 μl of the 14-3-3ζ–PKCεV3-pS346-pS368 complex, at a concentration of 42 mg/ml, was added to 1 μl 22% (w/v) polyethylene glycol 3350 (PEG3350), 100 mM calcium acetate, 50 mM NaF and incubated at 20 °C for 4 weeks. The crystals were crushed and seeded in sitting drops

with 1 µl of protein complex at 32 mg/ml and 1 µl 18% (w/v) PEG3350, 50 mM calcium acetate, 50 mM NaF and incubated at 20 °C for 2 weeks to give diffraction quality crystals. The crystals were soaked step-wise in a final solution of 10% (v/v) glycerol, 20% (w/v) PEG3350, 50 mM calcium acetate and 50 mM NaF before cryo-cooling in liquid nitrogen.

X-ray data collection and structural refinement. The native data set for 14-3-3ζ–PKCεV3-pS346-pS368 was collected to an effective resolution of 2.25 Å. The data were processed and scaled using XDS (Kabsch, 1988, 1993). Phaser (McCoy *et al*, 2007) was used for molecular replacement. Pseudo-merohedral twinning was detected using phenix.xtriage and least squares twin refinement was carried out using phenix.refine (Adams *et al*, 2002), with manual rebuilding carried out using Coot (Emsley & Cowtan, 2004). The coordinates have been deposited in the PDB with accession number 2WH0.

Supplementary information is available at *EMBO reports* online (http://www.emboreports.org).

ACKNOWLEDGEMENTS

Thanks to the Cancer Research-UK Peptide Synthesis Laboratory, to J. Endicott and J. Welburn for advice, and A. Aitken for the 14-3-3 cDNA. We also thank S. Mouilleron, J. Murray-Rust and E. Lorentzen for providing X-ray crystallography expertize, and R. George for help with the ITC data. We acknowledge support from EU FP6 #LSHB-CT-2004-503467.

CONFLICT OF INTEREST

The authors declare that they have no conflict of interest.

REFERENCES

Adams PD, Grosse-Kunstleve RW, Hung LW, Ioerger TR, McCoy AJ, Moriarty NW, Read RJ, Sacchettini JC, Sauter NK, Terwilliger TC (2002) PHENIX: building new software for automated crystallographic structure determination. *Acta Crystallogr D Biol Crystallogr* **58:** 1948–1954

Bridges D, Moorhead GB (2005) 14-3-3 proteins: a number of functions for a numbered protein. *Sci STKE* **2005:** re10

Delano WL (2002) *The PyMOL Molecular Graphics System*. Palo Alto, CA USA: Delano Scientific. http://www.pymol.org

Durgan J, Cameron AJ, Saurin AT, Hanrahan S, Totty N, Messing RO, Parker PJ (2008) The identification and characterization of novel PKCepsilon phosphorylation sites provide evidence for functional cross-talk within the PKC superfamily. *Biochem J* **411:** 319–331

Emsley P, Cowtan K (2004) Coot: model-building tools for molecular graphics. *Acta Crystallogr D Biol Crystallogr* **60:** 2126–2132

Fiol CJ, Wang A, Roeske RW, Roach PJ (1990) Ordered multisite protein phosphorylation. Analysis of glycogen synthase kinase 3 action using model peptide substrates. *J Biol Chem* **265:** 6061–6065

Fuglsang AT, Visconti S, Drumm K, Jahn T, Stensballe A, Mattei B, Jensen ON, Aducci P, Palmgren MG (1999) Binding of 14-3-3 protein to the plasma membrane H(+)-ATPase AHA2 involves the three C-terminal residues Tyr(946)-Thr-Val and requires phosphorylation of Thr(947). *J Biol Chem* **274:** 36774–36780

Ganguly S, Weller JL, Ho A, Chemineau P, Malpaux B, Klein DC (2005) Melatonin synthesis: 14-3-3-dependent activation and inhibition of arylalkylamine *N*-acetyltransferase mediated by phosphoserine-205. *Proc Natl Acad Sci USA* **102:** 1222–1227

Henriksson ML, Francis MS, Peden A, Aili M, Stefansson K, Palmer R, Aitken A, Hallberg B (2002) A nonphosphorylated 14-3-3 binding motif on exoenzyme S that is functional *in vivo*. *Eur J Biochem* **269:** 4921–4929

Kabsch W (1988) Evaluation of single-crystal X-ray diffraction data from a position-sensitive detector. *J Appl Cryst* **21:** 916–924

Kabsch W (1993) Automatic processing of rotation diffraction data from crystals of initially unknown symmetry and cell constants. *J Appl Cryst* **26:** 795–800

Kim JS, Diebold BA, Babior BM, Knaus UG, Bokoch GM (2007) Regulation of Nox1 activity via protein kinase A-mediated phosphorylation of NoxA1 and 14-3-3 binding. *J Biol Chem* **282:** 34787–34800

Liu D, Bienkowska J, Petosa C, Collier RJ, Fu H, Liddington R (1995) Crystal structure of the zeta isoform of the 14-3-3 protein. *Nature* **376:** 191–194

McCoy AJ, Grosse-Kunstleve RW, Adams PD, Winn MD, Storoni MC, Read RJ (2007) Phaser crystallographic software. *J Appl Cryst* **40:** 658–674

Muslin AJ, Tanner JW, Allen PM, Shaw AS (1996) Interaction of 14-3-3 with signaling proteins is mediated by the recognition of phosphoserine. *Cell* **84:** 889–897

Obsil T, Ghirlando R, Klein DC, Ganguly S, Dyda F (2001) Crystal structure of the 14-3-3zeta:serotonin *N*-acetyltransferase complex. A role for scaffolding in enzyme regulation. *Cell* **105:** 257–267

Obsil T, Ghirlando R, Anderson DE, Hickman AB, Dyda F (2003) Two 14-3-3 binding motifs are required for stable association of forkhead transcription factor FOXO4 with 14-3-3 proteins and inhibition of DNA binding. *Biochemistry* **42:** 15264–15272

Ottmann C *et al* (2007) Structure of a 14-3-3 coordinated hexamer of the plant plasma membrane H+-ATPase by combining X-ray crystallography and electron cryomicroscopy. *Mol Cell* **25:** 427–440

Peng CY, Graves PR, Thoma RS, Wu Z, Shaw AS, Piwnica-Worms H (1997) Mitotic and G2 checkpoint control: regulation of 14-3-3 protein binding by phosphorylation of Cdc25C on serine-216. *Science* **277:** 1501–1505

Petosa C, Masters SC, Bankston LA, Pohl J, Wang B, Fu H, Liddington RC (1998) 14-3-3zeta binds a phosphorylated Raf peptide and an unphosphorylated peptide via its conserved amphipathic groove. *J Biol Chem* **273:** 16305–16310

Rittinger K, Budman J, Xu J, Volinia S, Cantley LC, Smerdon SJ, Gamblin SJ, Yaffe MB (1999) Structural analysis of 14-3-3 phosphopeptide complexes identifies a dual role for the nuclear export signal of 14-3-3 in ligand binding. *Mol Cell* **4:** 153–166

Saurin AT, Durgan J, Cameron AJ, Faisal A, Marber MS, Parker PJ (2008) The regulated assembly of a PKCepsilon complex controls the completion of cytokinesis. *Nat Cell Biol* **10:** 891–901

Tzivion G, Luo Z, Avruch J (1998) A dimeric 14-3-3 protein is an essential co-factor for Raf kinase activity. *Nature* **394:** 88–92

Waterman MJ, Stavridi ES, Waterman JL, Halazonetis TD (1998) ATM-dependent activation of p53 involves dephosphorylation and association with 14-3-3 proteins. *Nat Genet* **19:** 175–178

Xiao B, Smerdon SJ, Jones DH, Dodson GG, Soneji Y, Aitken A, Gamblin SJ (1995) Structure of a 14-3-3 protein and implications for coordination of multiple signalling pathways. *Nature* **376:** 188–191

Yaffe MB (2002) How do 14-3-3 proteins work?—Gatekeeper phosphorylation and the molecular anvil hypothesis. *FEBS Lett* **513:** 53–57

Yaffe MB, Rittinger K, Volinia S, Caron PR, Aitken A, Leffers H, Gamblin SJ, Smerdon SJ, Cantley LC (1997) The structural basis for 14-3-3:phosphopeptide binding specificity. *Cell* **91:** 961–971

Zeng Y, Forbes KC, Wu Z, Moreno S, Piwnica-Worms H, Enoch T (1998) Replication checkpoint requires phosphorylation of the phosphatase Cdc25 by Cds1 or Chk1. *Nature* **395:** 507–510